

Investigation of helium addition for laser-induced plasma spectroscopy of pure gas phase systems: Analyte interactions and signal enhancement[☆]

C.A. Henry, P.K. Diwakar, D.W. Hahn^{*}

Department of Mechanical and Aerospace Engineering, University of Florida, Box 116300, Gainesville, FL 32611-6300

Received 10 March 2007; accepted 2 October 2007

Available online 9 October 2007

Abstract

The role of helium addition on the analyte signal enhancement in laser-induced breakdown spectroscopy for analysis of pure gaseous systems was examined using carbon and hydrogen atomic emission lines. Increased analyte response, as measured by peak-to-base and signal-to-noise ratios, was observed with increasing helium addition, with maximum enhancement approaching a factor of 7. Additional measurements revealed a significant decrease in plasma electron density with increasing helium addition. To explore the mechanisms of analyte signal enhancement, the helium emission lines were also examined and found to be effectively quenched with nitrogen addition. In consideration of the data, it is concluded that the role of metastable helium is not as important as the overall changes in plasma properties, namely electron density and laser-plasma coupling. Helium addition is concluded to affect the electron density via Penning ionization, as well as to play a role in the initial plasma breakdown processes.

© 2007 Elsevier B.V. All rights reserved.

Keywords: LIBS; Laser-induced plasma; Metastable

1. Introduction

Laser-induced breakdown spectroscopy (LIBS) has been widely explored for the analysis of solids, while less attention has been focused on the analysis of liquids, gases and aerosol samples. Nonetheless, some of the pioneering LIBS work was focused on aerosol analysis [1,2], and much of the early experimental and theoretical studies examined the laser-induced breakdown of gases [3]. In recent studies, LIBS has been applied to sample and analyze aerosol populations, including ambient air, using various implementations including single-shot analysis to take advantage of the discrete plasma volume [4–10]. However, gains in signal-to-noise ratios typically realized with ensemble averaging are not applicable with single-shot analysis, therefore it is important to maximize the signal and precision on a shot-to-shot basis [11,12]. For analysis of trace elements

contained within aerosol particles (e.g. analysis of single, aerosolized spores), the analyte mass of targeted elements may extend to the single fg level, which may be near or below the detection limits for single-shot LIBS [7]. Accordingly, to further establish single-shot LIBS-based techniques as an integrated analytical tool for detection and quantitative analysis of aerosols and dilute gaseous species, it is desirable to seek improvements in the precision and the overall method detection limit. In earlier studies, we have explored these goals in terms of the laser-plasma coupling [11], the laser pulse stability [13], and the use of double-pulse laser excitation [14]. In the current work, the effects of helium addition to the gaseous analyte sample stream are explored as a means to further improve the LIBS signal response.

The examination of helium use with laser-induced plasmas is not a new concept, with studies going back over two decades. Kuzuya et al. reported that emission line-to-continuum ratios were maximized in a reduced-pressure helium atmosphere for the analysis of several solid metals [15]. Time-resolved emission characteristics were explored for solid aluminum and copper targets, as well as with gas breakdown, for plasmas in helium [16]. They examined the roles of helium in energy transfer and

[☆] This paper was presented at the 4th International Conference on Laser Induced Plasma Spectroscopy and Applications (LIBS 2006) held in Montreal, Canada, 5–8 September 2006, and is published in the Special Issue of Spectrochimica Acta Part B, dedicated to that conference.

^{*} Corresponding author.

E-mail address: dwhahn@ufl.edu (D.W. Hahn).

corresponding signal enhancement, concluding that metastable helium can act as a significant energy reservoir, providing energy for ionization and excitation of excited states. Brust et al. performed detailed measurements of the collision cross-sections for Mg and Ca ions in a helium buffer gas during the laser ablation of solid samples, including comparisons with theoretical treatment [17]. Lee et al. also explored the roles of helium as a cover gas for laser-induced plasma analysis of copper targets, discussing the relative effects of ionization potential and diffusion coefficients on the resulting analyte signal [18]. More recently, Tran et al. used LIBS for analysis of halogens in organic solids for various buffer gases [19]. Helium was found to produce the optimal signal-to-noise ratio in comparison to air and argon, and resulted in reduced line broadening. Contemporary studies by Kurniawan and co-workers have specifically addressed the role of helium for enhancement of hydrogen analysis in solid samples, including zircaloy-4 alloys, via the LIBS technique [20–24]. In their studies, hydrogen emission intensities were enhanced while Stark broadening was reduced through the use of helium breakdown, using both single and double-laser LIBS methodologies. They attribute their findings to direct excitation of hydrogen emission from metastable excited state helium atoms.

In related studies other than laser-induced plasmas, Wagatsuma and Hirokawa have studied the effects of helium addition in a glow discharge reactor by analysis of the Ar II emission lines [25]. They found that when the excitation energy of the Ar II lines was less than the internal energy of the helium metastable states, the intensity of the Ar II lines were significantly increased, while in contrast, they found a reduction in emission intensity when the excitation energy exceeded the He metastable state. Helium has also been used and studied in microwave-induced plasmas [26–31]. As an example, Clay and Niemczyk have studied the effects of metastable energy transfer for metastable nitrogen, and reported that at nitrogen concentrations above 3%, the influence of metastable nitrogen is quite significant [26]. In a more recent paper, Naveed et al. examined the effects of helium gas mixing on production of active species in nitrogen plasmas [31]. They specifically discuss the role of metastable helium in energy transfer to molecular nitrogen via the Penning effect in the context of the relative energy states.

While the above studies are by no means intended to be a comprehensive review of the relevant literature, in concert, they

do suggest the careful investigation of helium addition for analysis of purely gas phase analyte systems, pursuant to the analysis of aerosol systems. Regarding aerosol analysis in particular, one must be careful to consider the decoupling of changes in bulk plasma properties as compared to effects limited to regions about individual particles. For example, the robustness of the gas-phase laser-induced breakdown process is often attributed to studies by Yalcin and co-workers, in which the overall plasma temperature and electron density were found to be remarkably independent of gas composition, including comparable plasma conditions for nitrogen, helium with 15% nitrogen, sulfur hexafluoride with 14% nitrogen, humidified nitrogen, and a nitrogen magnesium aerosol [32,33]. However, recent measurements of single aerosol particles in laser-induced plasmas reveal that plasma–particle interactions are confined to relatively small regions within the larger plasma volume [34], hence the potential to impact analyte signals independent of the overall plasma parameters is intriguing. With these comments in mind, the current study is focused on detailed analysis of the effect of helium addition on the analytical figures of merit and related plasma properties for analysis of purely gas-phase systems.

2. Experimental methods

A Q-switched Nd:YAG (Continuum Precision II) laser operating at its fundamental wavelength of 1064 nm and at a repetition rate of 5 Hz was used for all experiments. A schematic of the optical configuration is shown in Fig. 1. A laser beam energy of 320 mJ/pulse (pulse-to-pulse stability less than 0.5% RSD) was used for all experiments. The laser beam was focused to the center of the sample chamber (a five-way vacuum cross) using a UV-grade plano-convex lens with 100-mm focal length. The laser pulse energy was sufficient to create a laser-induced breakdown for every laser pulse over all gas compositions explored.

Spectral emission from the laser-induced plasma was collected via backscatter using a pierced mirror and focused onto a fiber optic bundle, as shown in Fig. 1, and subsequently coupled to the spectrometer. The light was then dispersed by the 0.275-m spectrometer (Acton SpectraPro-275) and finally recorded by a 256×1024 element intensified CCD array. The spectrometer used a 2400 groove/mm grating, which provided an

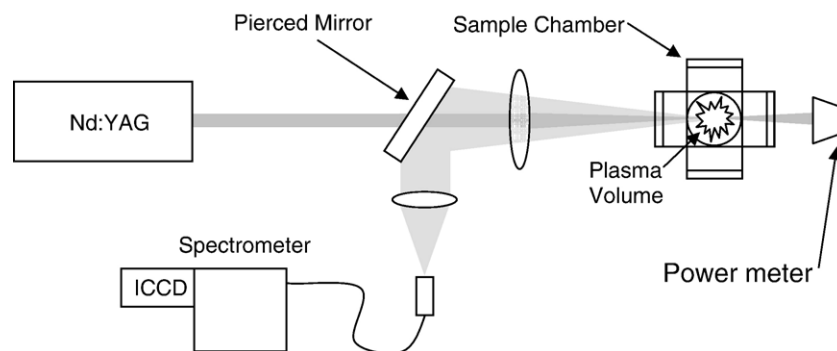


Fig. 1. Experimental set-up for LIBS measurements, showing the power meter in place for transmission measurements.

approximately 30-nm wavelength range with 0.12 nm spectral resolution. For all experiments, the external Q-switch sync from the laser was used to trigger the ICCD controller. Hence for each given set of experiments, the ICCD was fixed relative to the temporal position of the laser. The ICCD gate (i.e. detector delay and width) was then synchronized to the laser, which allowed for optimization of the specific atomic emission signals.

2.1. Carbon and hydrogen spectral measurements

For the carbon and hydrogen spectral measurements, a constant flow rate of 25 cc/min of methane was mixed with a 10 lpm (total flow) mixture of nitrogen and helium. The methane served as the source of elemental carbon and hydrogen in the plasma. The nitrogen and helium flow rates were varied from pure nitrogen to pure helium using 2.5 lpm increments. In this manner, the percentage of methane was held constant at 0.25%, while the percentage of helium in the balance was varied from 0 to 100%. It is noted that throughout the manuscript, the percentage of helium and nitrogen refer to the bulk 10 lpm flow, and do not reflect the 0.25% of methane that is held constant. The carbon and hydrogen lines were then analyzed as a function of gas composition. For the carbon line detection at 247.86 nm, an ICCD gate delay of 9 μs and gate width of 0.75 μs was used; hence spectral integration was initiated 9 μs following plasma initiation, which is coincident with the laser pulse. For the hydrogen line detection at 656.28 nm, an ICCD gate delay of 5 μs and gate width of 0.15 μs was used.

Spectral data were acquired using an ensemble average of 250 laser shots. All measurements were repeated a total of six times for both the carbon and hydrogen emission lines. To explore temporal signal optimization, a second set of spectral data was taken while varying the gate delay for both the carbon and hydrogen emission lines. For these measurements, the delay was varied from 3 μs to 18 μs over six equally spaced delay intervals. To avoid detector saturation over the full range of delay times, the detector gate widths were reduced to 0.5 μs and 0.125 μs for the carbon and hydrogen analysis, respectively. These measurements were repeated for each of the full range of helium and nitrogen mixture percentages used for the previous experiments.

2.2. Helium emission quenching measurements

Spectral analysis was also used to quantify the signal quenching effect of nitrogen on both the 587.87 and 388.87-nm helium emission lines. For the quenching measurements, helium flow was maintained at a constant rate of 10 lpm, while a nitrogen flow rate was varied from 0 to 5 lpm. Data were collected for eleven different flow rates of nitrogen while the He emission lines were recorded using a 250-shot ensemble average. For both the 587.87 and 388.87-nm helium emission lines, data were collected using two different detector gate delays and gate widths, namely for the same delay (9 μs) and width (0.75 μs) used for the carbon analysis, and for the same delay (5 μs) and width (0.15 μs) used for the hydrogen analysis.

Additional neutral density filters were placed in front of the fiber optic as necessary to attenuate the pronounced He emission lines so that detector saturation was avoided. Optical densities of 2.3 and 1.6 were used for the delays of 9 and 5 μs , respectively. Finally, an additional set of measurements was performed over the same range of flow conditions, during which the 656.28-nm hydrogen emission line was recorded. While the same helium and nitrogen flow rates were utilized, a constant hydrogen flow rate of 10 cc/min was added to the flow to seed the mixture with hydrogen. The 0.1% hydrogen flow was found to have no influence on the helium emission line intensities. Hydrogen emission was recorded at 656.28 nm using a delay of 5 μs and width of 0.15 μs . No neutral density filters were required for this set of data.

2.3. Transmission measurements

To assess the amount of laser pulse energy deposited into the laser-induced plasma, transmission experiments were performed. Laser pulse energy measurements were made for the laser at a spatial location directly in front of the sample chamber (i.e. incident energy) and at a location directly exiting the sample chamber (i.e. transmitted energy). A volume-integrating laser energy meter was used for these measurements, with the detector head placed directly in front of the five-way cross for incident beam measurements, and immediately after the chamber to measure the transmitted laser beam energy. The latter configuration is shown in Fig. 1. The average transmitted energy was then calculated from the direct ratio of these two measurements, making corrections for laser transmission through the chamber windows and lens. The transmission measurements were recorded for the quenching measurement flow concentrations, and for the spectral analysis flow concentrations. All transmission measurements were repeated a minimum of three times each.

3. Results and discussion

3.1. Analysis of carbon and hydrogen emission

Experiments were performed to determine the influence of helium addition on the analyte signal in a purely gas-phase system following laser-induced plasma formation. The laser pulse energy was fixed at 320 mJ/pulse, which was sufficient to create a robust plasma formation in either pure helium or pure nitrogen flows, as described above. The analyte signals were the carbon neutral emission line at 247.86 nm (24,648–61,982 cm^{-1}) and the hydrogen alpha emission line at 656.28 nm (82,259–97,492 cm^{-1}). As discussed above, both the hydrogen and carbon atoms were obtained from the dissociation of methane, which was kept at a constant concentration of 0.25% (volume) while the nominal percentage of helium was varied from 0 to 100%, in a balance of nitrogen. The H_α atomic emission line intensity was recorded at a delay time of 5 μs following plasma initiation using a detector gate of 0.15 μs . These gating conditions generally correspond to the optimal detection conditions for hydrogen analysis. Because the H_α line is considerably broadened,

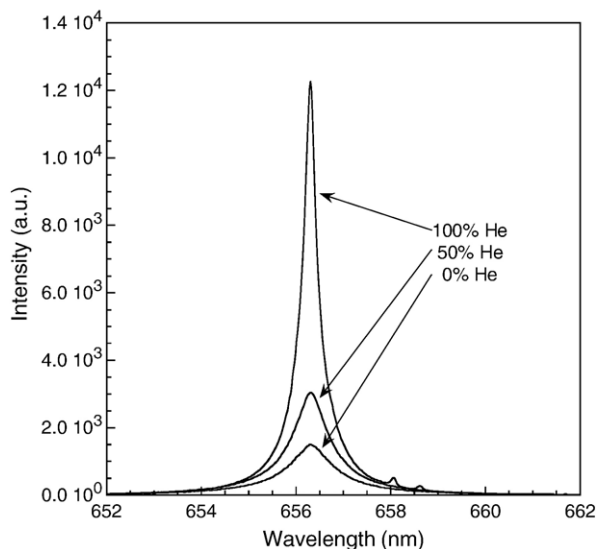


Fig. 2. Hydrogen (656.28 nm) emission spectra (background subtracted) recorded for various concentrations of helium in a nitrogen balance. Spectra were recorded at a time delay of 5 μ s, and are all presented with the same intensity scale.

and given the significant structure in the continuum emission, blank spectra were recorded for each helium–nitrogen combination (i.e. no methane). These blank spectra were then scaled to the hydrogen-containing spectra to enable accurate calculation of the integrated hydrogen peak using background subtraction. The peak-to-base (P/B) ratios were then calculated using the scaled blank for continuum emission intensity, and the signal-to-noise ratios (SNR) were calculated by evaluating the RMS spectral noise on either side of the hydrogen peak and averaging the results.

Representative hydrogen emission spectra are presented in Fig. 2 for pure nitrogen, pure helium, and a 50–50 mixture of

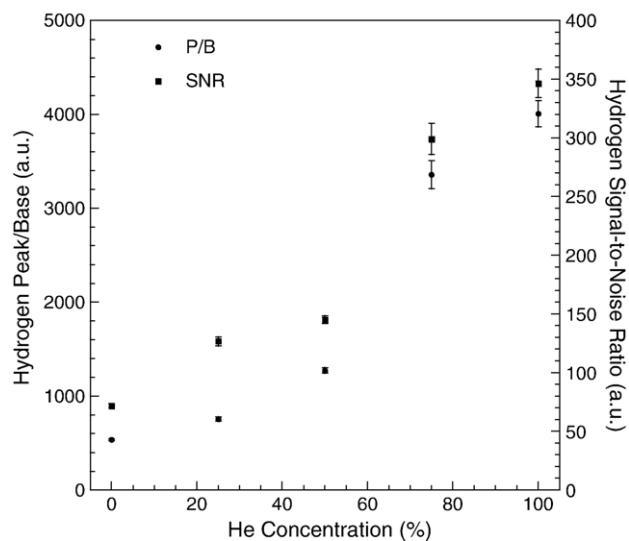


Fig. 3. Hydrogen emission signals (P/B and SNR of the 656.28-nm line) as a function of helium concentration in a balance of nitrogen. Error bars represent one standard deviation.

the two. Several key features are observed in the figure, namely, that the H_{α} emission line is significantly enhanced with increasing helium concentration, and that the line width (fwhm) is diminished with increasing helium concentration. The continuum emission is much weaker than the atomic emission lines, but was comparable for all gas concentrations. To assess the degree of hydrogen enhancement with helium addition, the analytical figures of merit (P/B and SNR) were calculated and are presented in Fig. 3. The data show a clear trend of increasing P/B and SNR with helium addition. Specifically, the hydrogen P/B is increased from 536 (2.2% RSD) in pure N_2 to 4008 (3.5% RSD) in pure He for an enhancement of 650%, while the SNR increased from 72 (2.1% RSD) in pure N_2 to 347 (3.4% RSD) in pure He for an enhancement of 380%.

The enhancement in hydrogen emission is consistent with previous research as discussed above, although the exact mechanism of signal increase remains to be determined. To assist in such a determination, it is useful to quantify the degree of Stark broadening in terms of the corresponding free electron density. The fractional half-widths used to reduce the Stark broadening data were those reported by Griem [35], assuming a plasma temperature of 15,000 K, which is appropriate for the delay times and laser pulse energy used [36]. The inversion of electron densities from Stark widths is rather insensitive to temperature, as related to the corresponding reduced line widths. Nonetheless, to assess sources of error due to temperature uncertainty in the present data, the measured Stark line widths were also inverted using temperatures of 10,000 and 20,000 K and the corresponding fractional half-widths. Accordingly, the uncertainties reported with the measured free electron densities represent the maximum error associated with the uncertainty of 5000 K, and the uncertainty associated with the measured line width (~ 0.02 nm). The calculated plasma electron densities as a function of helium composition are presented in Fig. 4. The analysis revealed that the free electron densities decay from $1.3 \times 10^{17} \text{ cm}^{-3}$ in pure nitrogen to $3.1 \times 10^{16} \text{ cm}^{-3}$ in pure

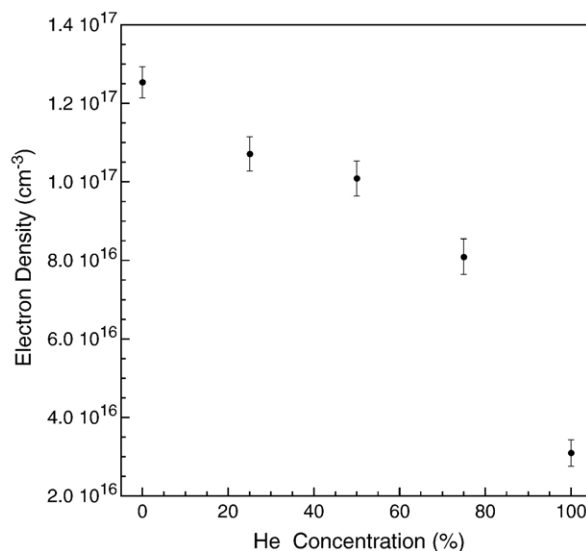


Fig. 4. Plasma electron density measured from Stark broadening as a function of helium concentration in a balance of nitrogen.

helium, a decrease of 75%. Such a decrease indicates that fundamental changes within the plasma are occurring, and these changes are consistent with the higher ionization potential of helium as compared to nitrogen (1402.3 kJ/mol for nitrogen and 2372.3 kJ/mol for helium).

The above measurements and analyses were repeated using the 247.86-nm carbon emission line. For carbon analysis, the delay was extended to 9 μ s (0.75 μ s width), which was closer to the optimal value. The relatively smooth nature of the continuum emission in the vicinity of the carbon line made the use of background subtraction unnecessary, and linear interpolation of the continuum emission was used for peak integration and baseline normalization. Representative spectra are presented in Fig. 5. The behavior of the carbon spectra is somewhat different than the hydrogen spectra discussed above. First, there is not a monotonic increase in carbon emission intensity with increasing helium concentration, as it is noted that the signal intensity for pure nitrogen exceeds the value for 50% helium. In fact, the absolute carbon signal strength was found to steadily decay with increasing helium concentration to a minimum at 75% helium, and to then increase to a maximum at 100% helium. Note also that the continuum emission in Fig. 5 is observed to increase as the helium concentration is increased. Finally, the linewidth of the carbon line was found to be essentially constant at 0.14 nm (0.8% RSD), which reflects the relative insensitivity of this line to Stark broadening. To again quantify the analyte response, the P/B and SNR values were calculated as a function of helium concentration, with the results presented in Fig. 6. These metrics once again display trends similar to the hydrogen analysis, namely an increasing value with increasing helium concentration. The carbon P/B is increased from 79 (5.0% RSD) in pure N₂ to 248 (5.6% RSD) in pure He for an enhancement of 213%, and the SNR increased from 260 (9.6% RSD) in pure N₂ to 540 (18% RSD) in pure He for an enhancement of 106%.

The above results support an analyte enhancement for both carbon and hydrogen anywhere from a factor of 2 to more than a

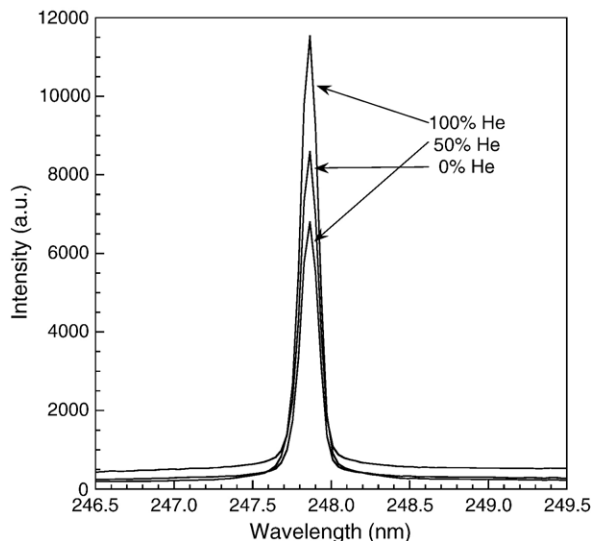


Fig. 5. Carbon (247.86 nm) emission spectra recorded for various concentrations of helium in a nitrogen balance. Spectra were recorded at a time delay of 5 μ s, and are all presented with the same intensity scale.

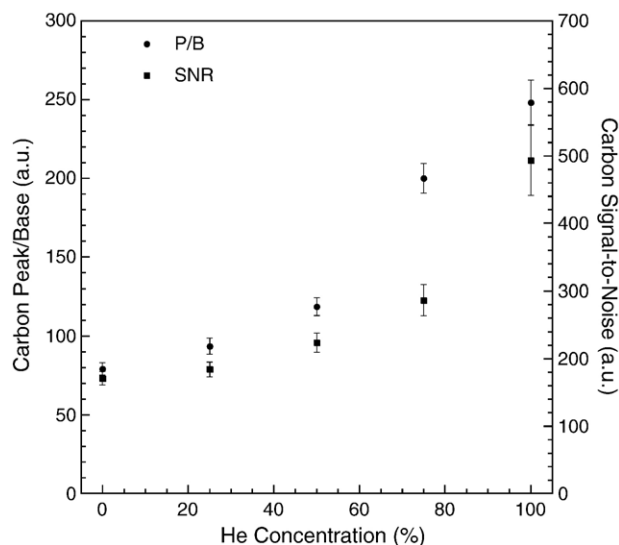


Fig. 6. Carbon emission signals (P/B and SNR of the 247.86-nm line) as a function of helium concentration in a balance of nitrogen. Error bars represent one standard deviation.

factor of 6 with increasing helium concentration. In addition, the plasma electron densities are observed to decrease with helium addition, which raises several additional questions. It is noted that the temporal gates were selected close to the optimal values for each of the analyte lines, namely a delay of 5 μ s for hydrogen analysis, and a delay of 9 μ s for carbon analysis. It is well known that the atomic emission response for each element and corresponding emission line has an optimal temporal delay that maximizes the signal, generally expressed in terms of the P/B or SNR ratios. One possible contributing factor to the data obtained above is a shift in the temporal decay profiles of the plasma, such that the addition of helium shifts the analyte emission to a more optimal value at the fixed delay times utilized. Because the pure nitrogen data were collected close to the optimal values (a detailed optimization was not initially performed), such a scenario may contribute to the observed effects and was therefore investigated. The temporal dependence of the 247.86-nm carbon emission SNR for the various helium/nitrogen compositions is presented in Fig. 7. While the carbon SNR in pure nitrogen is near the optimal value for the 9 μ s delay utilized for the Fig. 6 data, the addition of helium is observed to somewhat alter the temporal behavior of the SNR values, with a marked change in the optimal value realized for pure helium. The conclusions drawn from the Fig. 6 data remain essentially unchanged in view of the Fig. 7 data with the exception of the pure helium case, for which the optimal delay produces a carbon enhancement of nearly 400% at the optimal value as opposed to the 106% enhancement realized at the non-optimal delay of 9 μ s for pure helium. The same analysis was performed for the H α atomic emission line, although the findings were not as significant. For all gas compositions, including pure helium and pure nitrogen, the optimal hydrogen SNR was at or very near the delay of 5 μ s used for the Fig. 3 measurements; hence consideration of the optimal temporal gating for each gas flow composition changed the reported enhancement factors by less than 10%.

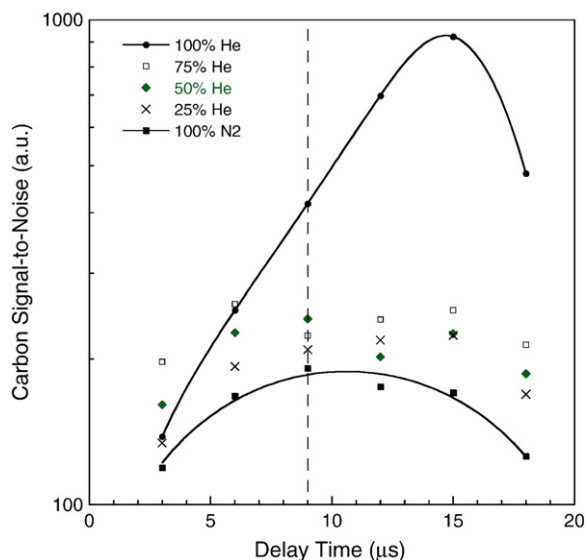


Fig. 7. Carbon emission signals (SNR of the 247.86-nm line) as a function of detector delay with respect to plasma initiation for various helium concentrations. The dashed line represents the delay used for the Fig. 5 data.

3.2. Analysis of helium emission: quenching effects and laser coupling

While the data and analysis presented above reveal significant enhancements in gas-phase analyte signals with increasing helium concentration, it is useful to also consider the behavior of the helium atomic emission as a means to gain insight into the actual enhancement mechanisms. Helium emission was analyzed using the 388.87 nm ($159,856\text{--}185,565\text{ cm}^{-1}$) and the 587.57 nm ($169,087\text{--}186,102\text{ cm}^{-1}$) neutral emission lines. The spectral intensity of both emission lines was pronounced for the case of pure helium, and as noted above, neutral density filters were added to eliminate detector saturation. However, the addition of

25% nitrogen, the lowest concentration investigated above, was found to essentially eliminate the observed helium emission lines. With this in mind, the effect of nitrogen addition on the helium emission lines was investigated over a range of nitrogen concentrations from 1 to 33% nitrogen in the helium balance. The helium emission intensity of the 388.87 and 587.57 lines is shown in Fig. 8 as a function of nitrogen concentration (helium balance), in which the P/B intensities have been normalized to the corresponding values in pure helium. The effect of nitrogen on the helium emission intensity is quite remarkable, with both helium emission lines essentially quenched completely with a nitrogen concentration of 33%. This effect was checked for other helium lines, and the same behavior was observed for the 402.6 nm ($169,087\text{--}193,917\text{ cm}^{-1}$), 447.1 nm ($169,087\text{--}191,445\text{ cm}^{-1}$), and the 501.57 nm ($166,278\text{--}186,210\text{ cm}^{-1}$) lines, namely complete quenching by 33% nitrogen concentration. To determine if this pronounced quenching of the helium transitions was unique to nitrogen, qualitative measurements were performed for other gases, checking to see if the helium lines vanished with approximately 33% added buffer concentration. The near identical behavior was observed for the addition of methane, hydrogen, carbon dioxide, and oxygen, noting that with 33% oxygen, the helium lines were reduced by about 90% rather than completely quenched.

To gain further insight into the observed analyte enhancements with helium addition, as well as the strong helium quenching observed above, two additional sets of measurements were performed. First, the 100% helium flow was seeded with 0.1% hydrogen, which was determined to produce essentially no quenching of the helium lines, and the quenching conditions were then repeated over the range of nitrogen concentrations while the H_{α} line was recorded for Stark broadening analysis. Secondly, the transmission of the laser pulse energy through the sample cell (i.e. through the plasma) was recorded to determine the quantity of laser energy coupled into the plasma as a function

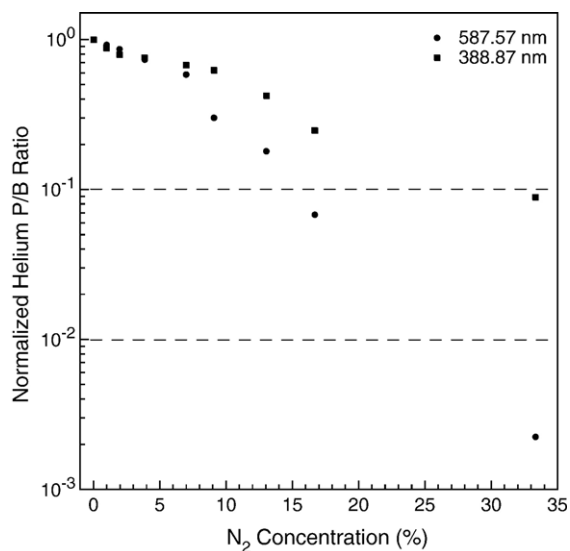


Fig. 8. Helium emission intensities of the 587.57 and 388.87-nm lines are presented as a function of nitrogen concentration in a helium balance. Both lines are normalized to the respective intensity values corresponding to pure helium.

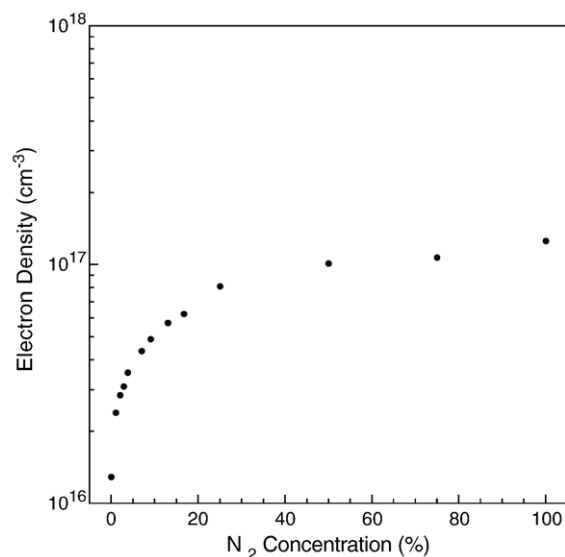


Fig. 9. Plasma electron density measured from Stark broadening as a function of nitrogen concentration in a balance of helium.

of gas composition. The results of the Stark broadening measurements are presented in Fig. 9 as the plasma electron density, and the results of the transmission experiments are presented in Fig. 10. Figs. 9 and 10 reveal consistent trends with regard to electron density and the amount of laser pulse energy coupled into the plasma, namely, a marked increase in both quantities with nitrogen addition. The two effects are self-consistent, in that the addition of relatively minor amounts of nitrogen results in a significant decrease in breakdown threshold due to the reduced ionization potential. It follows that the breakdown process is initiated earlier into the laser pulse temporal profile, resulting in additional energy being coupled into the plasma, and a concomitant increase in electron density. These comments notwithstanding, one must consider the data of Figs. 8–10 in the context of analyte emission enhancement with increasing helium concentration rather than increasing nitrogen concentration. From this point of view, it is not readily apparent why moving from right to left across curves in Figs. 9 and 10 results in a significant increase in analyte emission, especially for such high upper energy states as the 247.86-nm carbon line ($61,982\text{ cm}^{-1}$) and the 656.28-nm hydrogen line ($97,492\text{ cm}^{-1}$). The fact that the emission intensity of these lines is increasing while the overall plasma input energy and electron density are decreasing, suggests that additional excitation schemes via the helium atoms should be explored.

3.3. Potential energy transfer mechanisms with helium

The role of helium addition in the observed analyte signal enhancement has several possible explanations. The recent work by Kurniawan and co-workers has specifically addressed this issue for hydrogen analysis via LIBS [20–24]. Similar to the current results, they observed an increase in hydrogen emission intensities combined with a decrease in hydrogen line broadening with helium addition, in which the latter may be

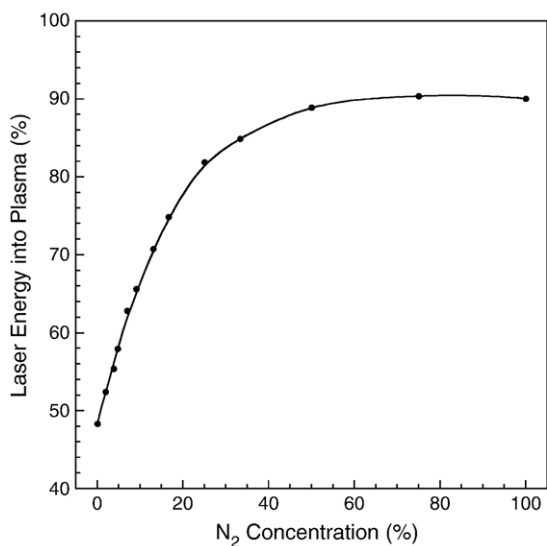


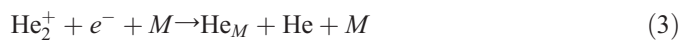
Fig. 10. Laser pulse energy (as a percentage of incident pulse energy) coupled into the plasma as a function of nitrogen concentration in a balance of helium. The incident laser pulse energy was 320 mJ.

interpreted as a decrease in electron density although no direct electron density calculations were reported. They attribute their findings to excitation of the hydrogen upper states via energy transfer from metastable state helium atoms, and discuss the competition between non-radiative energy transfer from the helium metastable and helium atomic emission from the metastable state. However, it is noted here that the energies of the helium metastable states are very high, namely $159,856\text{ cm}^{-1}$ for the 2^3S metastable and $166,278\text{ cm}^{-1}$ for the 2^1S metastable. As reported in Wagatsuma and Hirokawa [25], the excitation of Ar II via metastable helium energy transfer was well explained for good matches in the excitation energy levels to the metastable states, as well as conservation of total spin. In contrast, the mismatch between metastable He and the hydrogen and carbon lines in the present study is considerable. In fact, no lines with comparably low energy levels realized appreciable emission enhancement with helium addition in the Wagatsuma and Hirokawa study. Therefore, direct excitation of the H_α line ($97,492\text{ cm}^{-1}$) via direct energy transfer from metastable helium does not appear important given the resulting excess energy. Similar comments are offered with regard to direct excitation of the carbon lines.

Given the above discussion, the direct role of metastable helium on the carbon and hydrogen analyte signals must be further considered in terms of the helium emission signals. The five helium lines examined in this study are all excited from pathways arising from the metastable states: including the 388.87-nm line which terminates in the 2^3S metastable state, the 587.57-nm line that terminates in the 2^3P state, which itself is coupled to the 2^3S metastable, and the 402.6 nm, 447.1 nm, and the 501.57 nm lines which arise from the 5^3D , 4^3D , and 3^3D states, respectively, and all terminate in the 2^3P state. The most probable explanation for the strong quenching of all these states is the quenching of the metastable states themselves. Collisional de-excitation of the metastable state He_M has been extensively studied, and is referred to as the Penning ionization



Penning ionization is prominent in helium plasma systems with the addition of nitrogen, as well as other gases, and is in excellent agreement with the present experimental results. As the nitrogen content is increased, the electron density is enhanced and the helium emission lines described above are eliminated as the metastable helium atoms are quenched to the ground state. Alternative schemes may be important, although the collisional deexcitation is the most logical. While electron impact is perhaps the dominant mechanism of formation of metastable helium in laser-induced plasmas, dissociative recombination of the molecular helium ion can play a role



However, direct dissociative recombination for formation of the metastable state is orders of magnitude more efficient when

the molecular helium ion is in an excited vibrational state [37]. The addition of nitrogen or other third bodies can reduce the molecular helium ion to its lowest vibrational state, thereby reducing the concentration of metastable helium through this formation path.

Regardless of the exact mechanisms, a conclusion of the present work is that the concentration of metastable helium in mixtures other than nearly pure helium is effectively quenched and therefore, the direct transfer of energy from metastable helium states to the analyte is perhaps not the most important path. However, it is worth noting that for cases of very low analyte concentrations in a helium balance, it is possible that metastable state helium atoms play a role in enhancement of analyte emission [24]. This is due to the fact that at very low analyte concentrations in a high helium balance, metastable helium has a significant population density, as observed in the present study (see Fig. 8). For the current carbon analysis, it is noted that the absolute carbon signal increased and then decreased with increasing helium concentration before finally increasing markedly at a 100% helium balance. Although the peak-to-base and SNR both exhibited monotonic increases with helium addition, it is possible that the metastable helium plays a role at the highest helium concentration. Notwithstanding the above comments, a more likely explanation for the observed analyte emission enhancements observed with helium addition in the present study is a perturbation of the overall plasma conditions, namely a decrease in absorbed laser energy and a decrease in electron density. Such perturbations may shift the plasma toward more optimal conditions regarding atomic emission as compared to continuum emission processes (e.g. free-free and free-bound), yielding the observed increases in analytical figures of merit, namely the P/B and SNR.

In summary, the present work has examined the role of helium addition on the analyte signal enhancement in laser-induced breakdown spectroscopy of purely gaseous systems. Analyte enhancements were observed with increasing helium addition, based on the analytical figures of merit. The increases were significant in a nearly pure helium environment, but were on the order of a factor of 2 or 3 for helium concentrations of 50%. Careful examination of the helium emission lines and plasma electron densities leads to the conclusion that the role of metastable helium is not as important as the overall changes in bulk plasma properties, namely electron density, continuum emission, and plasma temperature. Helium addition affects the plasma electron density via Penning ionization, as well as the initial plasma breakdown processes and consequent plasma-laser coupling and energy absorption. The role of helium addition for aerosol analysis remains to be studied, but one must consider the overall effects of analyte dilution (and aerosol dilution) with helium addition. For example, a factor of two increase in analyte response, as was approximately realized for carbon analysis at a 50% helium concentration, would be offset by a factor of two analyte dilution if helium was simply added to the analyte sample stream. However, for single-shot aerosol analysis, dilution effects are not important provided the analysis is not limited by particle hit rates. For such applications, factors of 2 to 4 may be important for critical sensing application.

Acknowledgements

This work was supported in part by the National Science Foundation through grant CTS-0317410. The authors express their gratitude to Prof. Nico Omenetto (University of Florida) for helpful discussions on the roles of metastable helium energy transfer.

References

- [1] L.J. Radziemski, T.R. Loree, D.A. Cremers, T.M. Hoffman, Time-resolved laser-induced breakdown spectrometry of aerosols, *Anal. Chem.* 55 (1983) 1246–1252.
- [2] L.J. Radziemski, Review of selected analytical applications of laser plasmas and laser-ablation, *Microchem. J.* 50 (1994) 218–234.
- [3] D.A. Cremers, L.J. Radziemski, Chapter 1, laser-induced breakdown spectroscopy: fundamentals and applications, in laser-induced breakdown spectroscopy, in: A.W. Miziolek, V. Palleschi, I. Schechter (Eds.), Cambridge University Press, 2006.
- [4] D.W. Hahn, M.M. Lunden, Detection and analysis of aerosol particles by laser-induced breakdown spectroscopy, *Aerosol Sci. and Tech.* 33 (2000) 30–48.
- [5] J.E. Carranza, B.T. Fisher, G.D. Yoder, D.W. Hahn, On-line analysis of ambient air aerosols using laser-induced breakdown spectroscopy, *Spectrochim. Acta Part B* 56 (2001) 851–864.
- [6] B. Hettinger, V. Hohreiter, M. Swingle, D.W. Hahn, Laser-induced breakdown spectroscopy for ambient air particulate monitoring: correlation of total and speciated aerosol counts, *Appl. Spectrosc.* 60 (2006) 237–245.
- [7] P.B. Dixon, D.W. Hahn, On the feasibility of detection and identification of individual bioaerosols using laser-induced breakdown spectroscopy, *Anal. Chem.* 77 (2005) 631–638.
- [8] G.A. Lithgow, A.L. Robinson, S.G. Buckley, Ambient measurements of metal-containing PM_{2.5} in an urban environment using laser-induced breakdown spectroscopy, *Atmos. Environ.* 38 (2004) 3319–3328.
- [9] R.E. Neuhauser, U. Panne, R. Niessner, G.A. Petrucci, P. Cavalli, N. Omenetto, On-line and in-situ detection of lead aerosols by plasma-spectroscopy and laser-excited atomic fluorescence spectroscopy, *Anal. Chim. Acta* 346 (1997) 37–48.
- [10] M.H. Nunez, P. Cavalli, G. Petrucci, N. Omenetto, Analysis of sulfuric acid aerosols by laser-induced breakdown spectroscopy and laser-induced fragmentation, *Appl. Spectrosc.* 54 (2000) 1805–1816.
- [11] J.E. Carranza, D.W. Hahn, Sampling statistics and considerations for single-shot analysis using laser-induced breakdown spectroscopy, *Spectrochim. Acta Part B* 57 (2002) 779–790.
- [12] G.A. Lithgow, S.G. Buckley, Effects of focal volume and spatial inhomogeneity on uncertainty in single-aerosol laser-induced breakdown spectroscopy measurements, *Appl. Phys. Lett.* 87 (2005) 011501.
- [13] V. Hohreiter, A. Ball, D.W. Hahn, Effects of aerosols and laser cavity seeding on spectral and temporal, *J. Anal. Atom. Spectrosc.* 19 (2004) 1289–1294.
- [14] B.C. Windom, P.K. Diwakar, D.W. Hahn, Dual-pulse LIBS for analysis of gaseous and aerosol systems: plasma-analyte interactions, *Spectrochim. Acta Part B* 61 (2006) 788–796.
- [15] M. Kuzuya, H. Matsumoto, H. Takechi, O. Mikami, Effect of laser energy and atmosphere on the emission characteristics of laser-induced plasmas, *Appl. Spectrosc.* 47 (1993) 1659–1664.
- [16] M.R. Joseph, N. Xu, V. Majidi, Time-resolved emission characteristics and temperature profiles of laser-induced plasmas in helium, *Spectrochim. Acta Part B* 49 (1994) 89–103.
- [17] J. Brust, M. Movre, K. Niemax, Measurement and calculation of the fine-structure changing collision cross-sections in the Mg⁺ and Ca⁺ resonance states by helium, *Z. Phys., D At. Mol. Clust.* 27 (1993) 243–248.
- [18] Y. Lee, K. Song, H. Cha, J. Lee, M. Park, G. Lee, J. Sneddon, Influence of atmospheric and irradiation wavelength on the copper plasma emission induced by excimer and Q-switched Nd:YAG laser ablation, *Appl. Spectrosc.* 51 (1997) 959–964.

- [19] M. Tran, Q. Sun, B.W. Smith, J.D. Winefordner, Determination of F, Cl, and Br in solid organic compounds by laser-induced plasma spectroscopy, *Appl. Spectrosc.* 55 (2001) 739–744.
- [20] M. Pardede, H. Kurniawan, T.J. Lie, R. Hedwig, N. Idris, T. Kobayashi, T. Maruyama, Y.I. Lee, K. Kagawa, M.O. Tjia, Hydrogen analysis in solid samples using laser-induced helium plasma at atmospheric pressure, *J. Appl. Phys.* 98 (2005) 043105.
- [21] S.N. Abdulmadjid, M.M. Suliyanti, K.H. Kurniawan, T.J. Lie, M. Pardede, R. Hedwig, K. Kagawa, M.O. Tjia, An improved approach for hydrogen analysis in metal samples using laser-induced gas plasma and target plasma at helium atmospheric pressure, *Appl. Phys. B* 82 (2006) 161–166.
- [22] K.H. Kurniawan, K. Kagawa, Hydrogen and deuterium analysis using laser-induced plasma spectroscopy, *Appl. Spectrosc. Rev.* 41 (2006) 99–130.
- [23] K.H. Kurniawan, M. Pardede, R. Hedwig, Z.S. Lie, T.J. Lie, D.P. Kurniawan, M. Ramli, K.I. Fukumoto, H. Niki, S.N. Abdulmadjid, N. Idris, T. Maruyama, K. Kagawa, M.O. Tjia, Quantitative hydrogen analysis of zircaloy-4 using low-pressure laser plasma technique, *Anal. Chem.* 79 (2007) 2703–2707.
- [24] M. Ramli, K. Kagawa, S.N. Abdulmadjid, N. Idris, W.S. Budi, M.A. Marpaung, K.H. Kurniawan, T.J. Lie, M.M. Suliyanti, R. Hedwig, M. Pardede, Z.S. Lie, M.O. Tjia, Some notes on the role of meta-stable excited state of helium atom in laser-induced helium gas breakdown spectroscopy, *Appl. Phys. B* 86 (2007) 729–734.
- [25] K. Wagatsuma, K. Hirokawa, Excitation of singly ionized argon species in helium-matrix glow discharge plasma-role of the energy transfer from helium metastables, *Spectrochim. Acta Part B* 50 (1995) 109–125.
- [26] J. Clay, T. Niemczyk, Factors influencing iron excitation in nitrogen rare-gas microwave plasmas, *Spectrochim. Acta Part B* 47 (1992) 835–841.
- [27] W.R.L. Masamba, J.D. Winefordner, Analytical characteristics of a helium hydrogen capacitively coupled microwave plasma, *Spectrochim. Acta Part B* 48 (1993) 521–529.
- [28] A. Rodero, M.C. Quintero, A. Sola, A. Gamero, Preliminary spectroscopic experiments with helium microwave induced plasma produced in air by use of a new structure: the axial injection torch, *Spectrochim. Acta Part B* 51 (1996) 467–479.
- [29] A.E. Croslyn, B.W. Smith, J.D. Winefordner, A review of microwave plasma sources in atomic emission spectrometry: literature from 1985 to the present, *Crit. Rev. Anal. Chem.* 27 (1997) 199–255.
- [30] N.K. Podder, J.A. Johnson, C.T. Raynor, S.D. Loch, C.P. Balance, M.S. Pindzola, Helium line intensity ratio in microwave-generated plasmas, *Phys. Plasmas* 11 (2004) 5436–5443.
- [31] M.A. Naveed, A. Qayyum, A. Shujaat, M. Zakauallah, Effects of helium gas mixing on the production of active species in nitrogen plasma, *Phys. Lett. A* 359 (2006) 499–503.
- [32] S. Yalcin, D.R. Crosley, G.P. Smith, G.W. Faris, Influence of ambient conditions on the laser air spark, *Appl. Phys. B* 68 (1999) 121–130.
- [33] S. Yalcin, D.R. Crosley, G.P. Smith, G.W. Faris, Spectroscopic characterization of laser-produced plasma for in situ toxic metal monitoring, *Haz. Waste and Haz. Materials* 13 (1996) 51–61.
- [34] V. Hohreiter, D.W. Hahn, Plasma-particle interactions in a laser-induced plasma: implications for laser-induced breakdown Spectroscopy, *Anal. Chem.* 78 (2006) 1509–1514.
- [35] R. Griem, *Spectral Line Broadening by Plasmas*, Academic Press, New York, 1974.
- [36] V. Hohreiter, J.E. Carranza, D.W. Hahn, Temporal analysis of laser-induced plasma properties as related to laser-induced breakdown spectroscopy, *Spectrochim. Acta Part B* 59 (2004) 327–333.
- [37] J. Raud, M. Laan, M. Aints, . The influence of N₂ as a trace gas to HF capillary discharge in He, *J. Phys. D: Appl. Phys.* 39 (2006) 2724–2731.